ANNALS OF GEOPHYSICS, 68, 4, T441, 2025; doi:10.4401/ag-9248
OPEN ACCESS

Fault Characterization from Lineaments based on Magnetic Data: A Case Study of Magadi Geothermal Prospect, Kenya

Evance Odero[*,1], John Githiri[1], Maurice K'Orowe[1], Patel Jayanti[2]

(1) Jomo Kenyatta University of Agriculture and Technology, Physics Department, Nairobi, Kenya
(2) Technical University of Kenya, Centre for Earth Systems and Space Sciences, Nairobi, Kenya

Article history: received January 14, 2025; accepted April 20, 2025

Abstract

Fault characterization is a crucial aspect of exploring geothermal resources. Recent research approves lineament mapping as a useful tool in structural studies. It is largely problematic to decipher the lineaments that are specifically linked to faults, ridges, or other tectonic structures. The study aims to characterize faults from lineaments using magnetic data from the Magadi-Nguruman area, west of Lake Magadi within the Kenyan Rift system. The magnetic data was reduced to pole before lineament generation using the Center of Exploration Targeting (CET) processes and Euler Deconvolution. A rose diagram was used to determine the orientation of the 21 major lineaments. Seven cross-sectional slices across the lineaments provided the data for calculating Euler solutions for the linear magnetic anomaly sources. The obtained Euler plots delineated the approximate depth, dip angles, identity, and strike of the structures linked to the lineaments. The case study results characterized 80% of the generated lineaments as faults with a general strike in the N-S direction. The dipping angles of the detected faults ranged between 36° and 83°, with the majority dipping towards the southern basement of Lake Magadi. The depth ranges of the detected faults were between 0.25 km and 0.74 km. The trends observed in this work are consistent with the reported regional fault orientations, thus qualifying the protocol used in this work. Magadi-Nguruman is sufficiently faulted for a possible geothermal system near Lake Magadi.

Keywords: Fault characterization; Magnetic data; Lineaments; Geothermal Exploration; Magadi

1. Introduction

Geological lineament analysis is a proven technique for recognizing faults, lithological boundaries tectonic units, geomorphic relief, and seismically active zones, making them significant indicators of subsurface structures (Choi et al., 2016; Ahmadi and Pekkan, 2021). Identifying faults from lineaments requires a thorough analysis that integrates geological, geophysical, and remote sensing techniques. Using geophysical potential fields to generate lineaments is a desirable complement to the traditional satellite image approach. This makes the experience of subsurface structural characterization a little easier and more accurate.

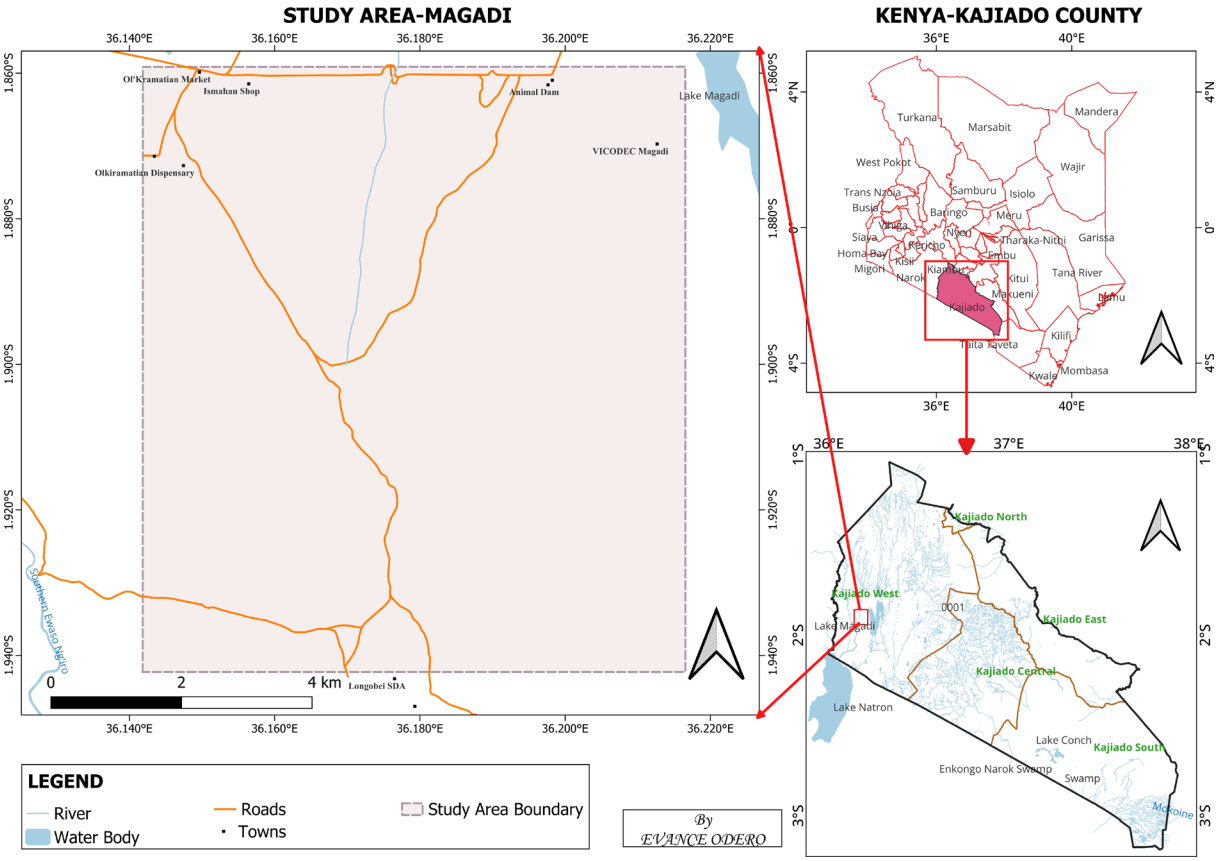

Figure 1. Topographical map of Magadi-Nguruman Study Area, Kajiado County, Kenya (Odero et al., 2024).

The Magadi area, west of Lake Magadi, falls within the Kenyan Rift System to the south. Figure 1 shows a 90 km^2 study area within the region, generally classified as the unexploited geothermal zone in Kenya (Omenda, 2014). The presence of geothermal surface manifestations such as hot springs and volcanic outcrops in the study area informed its case selection. The tectonic activities, and the subsurface volcanic dense bodies within the Rift System, are partly associated with geothermal heat sources, and can be linked to the fault patterns in the region. For geothermal exploration, the volcanic centers linked to cooling volcanic intrusion within the subsurface, are of great interest. These can be evidenced by surface manifestations such as hot springs which signify the presence of conduits such as faults (Mariita and Keller, 2007; Gentana, Sulaksana, Sukiyah, and Yuningsih, 2019; Abdullah, Puspita, and Hamad, 2020; Werff, 2024).

2. Geology

Kenya Rift System is part of the East African Rift System (EARS) which can be traced to worldwide mid-oceanic rift systems. It belongs to the eastern branch of EARS together with Afar, Ethiopia, and Turkana (Omenda, 2007). The stages of Kenyan rift formation began with tectonic updoming and volcanism on uplift crests, followed by half to full-graben faulting in the early Pleistocene. Basaltic and trachytic lava erupted and flowed over the floor and flanks as observed in places such as Mt. Longonot. These recent volcanic activities are inferred to have occurred about 140 years ago (Alexander, Ussher and Merz, 2011). The western Magadi area in Kajiado County falls within the Kenyan Rift to the south, with a similar geological setting. A model was developed (Muirhead et al., 2016; Simiyu and Keller, 1998) proposing an existing basement underneath Lake Magadi. The basement is exposed at the western and eastern flanks forming the Tanzania craton and Mozambique belt respectively, with evidence of faulting and lower-crust intrusions. The basement is overlain by Pliocene to Miocene volcanic and sedimentary rocks. Holocene sediments overlying widespread Pleistocene Trachyte lavas generally cover the broader Magadi area (Githiri, Patel, Barongo and Karanja, 2012).

More structural studies have inferred the presence of North-South trending faulted escarpments and a system that controls the occurrence of geothermal manifestations in the Magadi area and the zones extending towards the Nguruman escarpment (Riaroh and Okoth, 1994; Odero, Githiri, and K'Orowe, 2024). Magadi region exhibits distinct fault strike and dip characteristics which are influenced by regional rifting and seismicity. The primary faults are found to align predominantly in the near NW-SE direction. Faults and fractal analysis carried out by Gloaguen and others (2007), using remote sensing, demonstrated a significant relationship between the rifting mechanism within the Magadi crust and the general fault direction. Steeply dipping faults were found to be common in the area with small variations in the dip angles (Gloaguen et al., 2007). These faulting behaviors were shaped by structural fabrics inherited from the tectonic deformation patterns across the Magadi rift zone (Zou et al., 2023). The reported average of dip angles within the Magadi-Nguruman area is about 60°, with a fault extension rate of 0.4-0.7 millimeters per year (Muirhead et al., 2016; Owen et al., 2018). The interplay between magmatic activity and the reported faulting dynamics drives interest in the geothermal potential investigations in Magadi. Also, understanding these attributes provides essential information needed in the construction of stress models of the faulted zones.

Figure 2 shows the spread of geological units over the entire study area. The map indicates major faults oriented in the North-South direction with Lake Magadi to the east of the study area. The intensity of faulting in the area indicate active tectonism. The mapped escarpments align with the faulting patterns leading to the formation

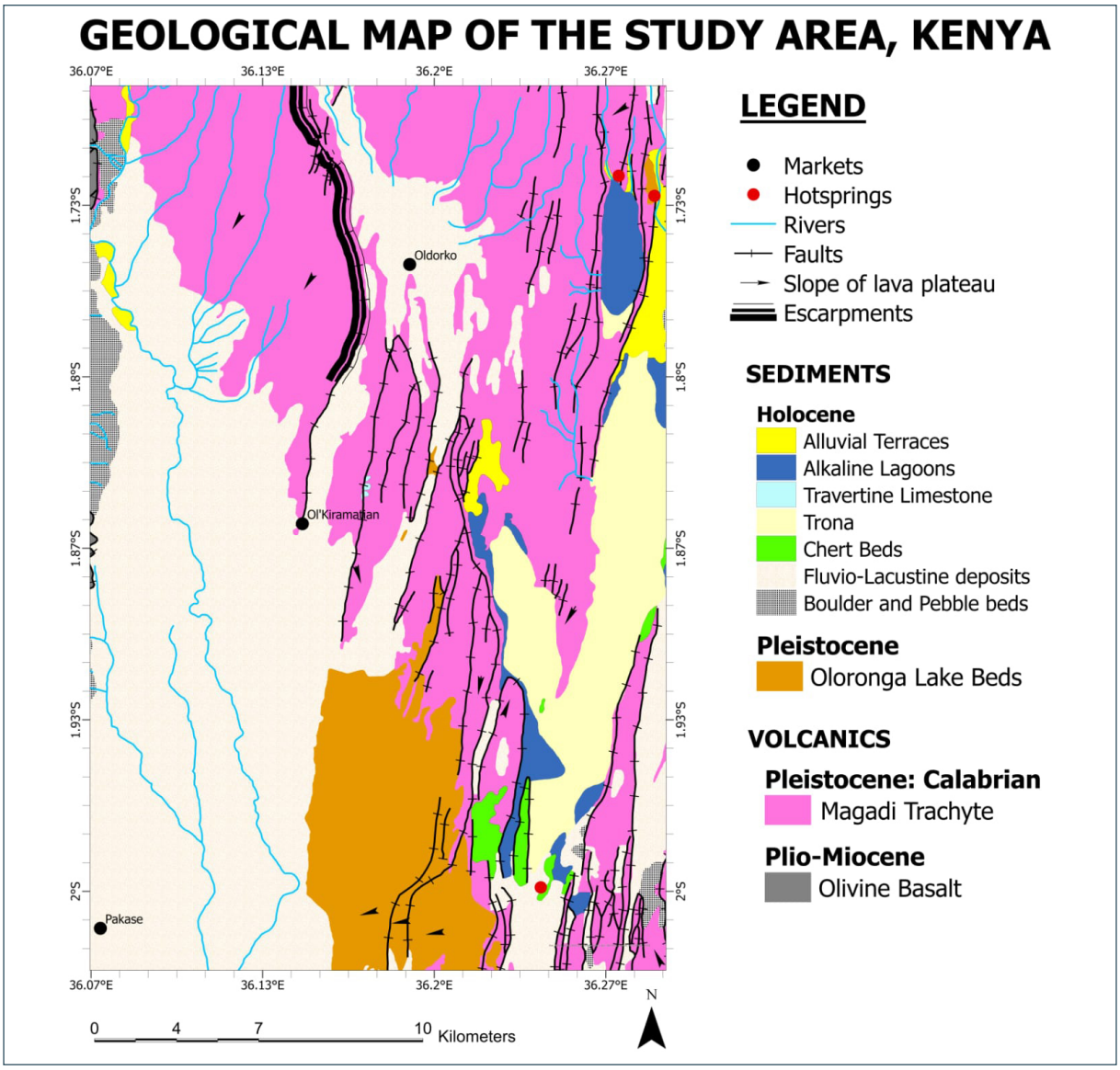

Figure 2. Main Geological units in the Magadi and Nguruman Zone.

of grabens and basins containing climatic and rift-related sediments such as the Holocene alluvial terraces, Fluvio-Lacutine deposits, boulders and pebbles (Githiri, Patel, Barongo and Karanja, 2011). The kind of sediments shown on the map infers possible environmental dynamics such as shrinking of lakes and rivers, flush floods, and volcanic activities. The abundance of the Lacustine sediments to the west of the study area can be associated with the activities of the Ewaso Ng'iro river and its tributaries. The presence of old Plio-Miocene Olive Basalts and Pleistocene Trachytes speaks to the volcanic history of the region. It represents a shift from ancient lava flows to a more silica-rich and explosive volcanism. The geochemistry of the Magadi Trachytes contributes to the salinity of the hydrological systems in the area (Getenet et al., 2020). The weathered trachytes also contribute to the formation of silicon-rich sediments that help sustain the saline environment for diatom flora in the lake (Owen et al., 2011). Widespread lava flows are evidenced by the lava plateau slopes (Muirhead et al., 2016). The units found in the Kajiado zone could be linked to marble and quartzite units of Taita Hills through nappe folds (Bauernhofer et al., 2000). Travertine Limestone forms from mineral-rich geothermal fluids as a result of calcium carbonate precipitation (Çetintaş, 2022). The tectonic activities in Magadi, including faulting and the subsequent opening of fissures, create pathways through which geothermal waters can rise and cool, facilitating precipitation. The stable flow rates observed in the Magadi region (Muirhead et al., 2016), likely enhanced by localized vegetation and soil characteristics, provide a conducive environment for the sustained deposition of Travertine Limestone. The association of the Holocene Limestones and the hot springs in Magadi provides vital information for the exploration of the geothermal potential of the region. Moreover, the map represents the hot springs as surrounded by silica-based Chert beds, additional evidence of the composition of the geothermal waters emitted by the hot springs. The deep-seated hot fluids reach the surface via faults. The fluid temperatures indicate a possibility of existing underlying magmatic heat sources.

The fault orientations determined in this study are significant for analyzing the rifting history, as well as the recharge and hot fluid pathways of a geothermal system (Utama, 2023; Abdullah, Puspita, and Hamad, 2020). The high rate of recent geothermal activity and volcanism related to geodynamic processes is clearly displayed in the Magadi region, indicating shallower structures that remain to be investigated in detail (Kuria, 2011). The established faults from lineaments exhibit characteristics that are consistent with the geology of Magadi.

3. Methodology

3.1 Magnetic Measurements

The instrument used to carry out ground magnetic measurement captured the total field $\boldsymbol{B}$ simply described by the inverse square relation shown by Eq. (1). The field $\boldsymbol{B}$ is directly related to the proton precession frequency f experienced by the protons within the instrument (Eq. (2)). The field varies inversely with the gyromagnetic γ_p of the proton (Shahsavani, 2018). The total field comprises the components of the anomalies.

$$B = \frac{\mu_0 m}{4\pi\mu_R r^2} \tag{1}$$

Where B is the field from the pole of magnetic strength m at distance r, μ_0 and μ_R are the magnetic permeability of free space and the relative magnetic permeability of the pole separation medium, respectively.

$$2\pi f = \gamma_p B \tag{2}$$

The 90 square kilometer study area was subdivided into twenty-one 9-km-long transects. Data stations, 250 m apart, were identified along the transects. A GSM 19 Proton Precession Magnetometer with a resolution of 0.01 nT was used to measure the total field values at stations. The station coordinates were determined using a differential GPS. 742 stations and several base station readings were captured, giving a station density of 8.244 stations per square kilometer. Figure 3 shows the distribution of data stations over the study area. Observable geologic features at the stations of measurement were noted.

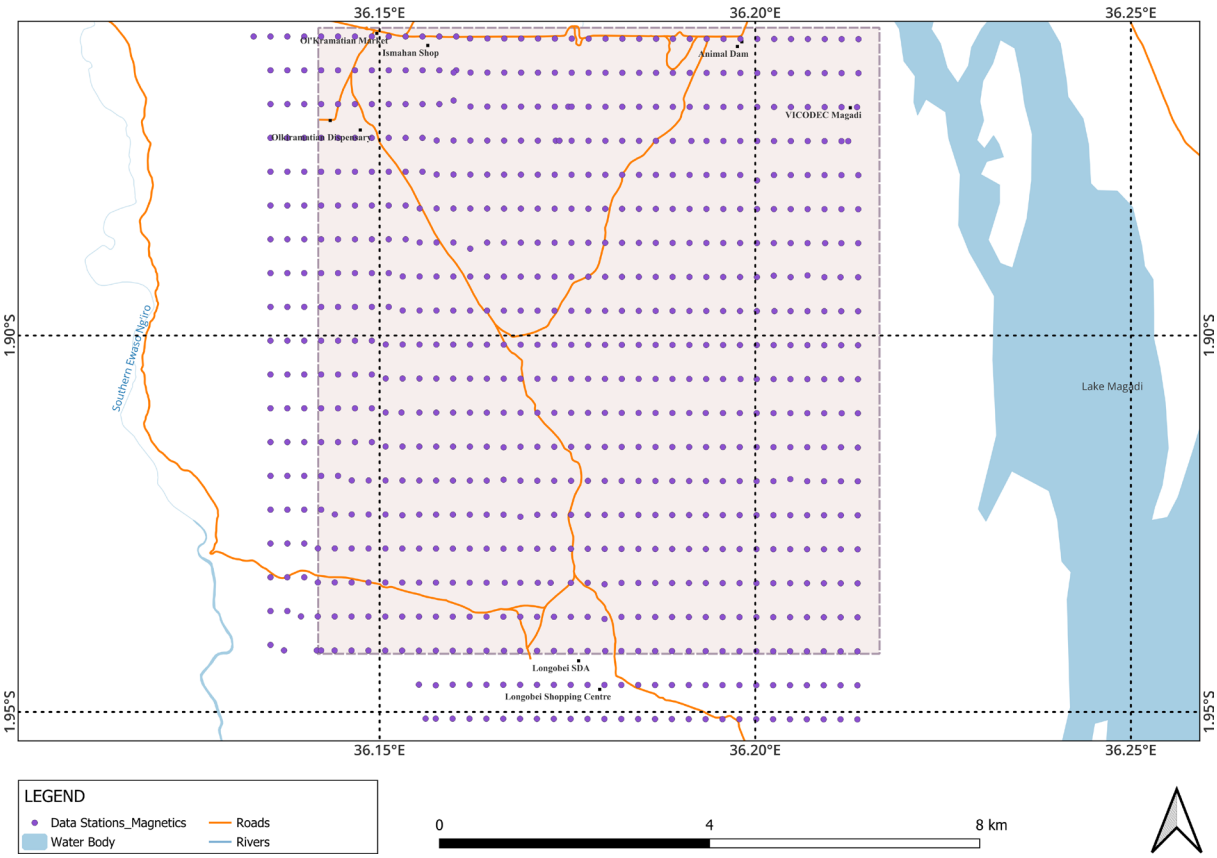

Figure 3. The Distributions of Magnetic Data Stations over the Study Area.

3.2 Magnetic Data Processing

Base station readings were used to correct for the diurnal variations in the magnetic data. Removal of the effect of the International Geomagnetic Reference Field (IGRF) was performed using the inclination and declination angles of −24.78° and 0.45°, respectively. High-pass filters were applied to remove the regional field. The resultant residual anomaly data was gridded for qualitative analysis. The contour map was overlain on Google Earth for the exact location and comparison with natural features. Lineament mapping using Magnetic data for Nguruman-Magadi was performed, and the corresponding Rose diagram for Lineaments was obtained. 2D Euler solutions for Fault depth and orientation investigations were conducted.

3.3 Lineament Generation

To develop lineaments from magnetic data, the magnetic residual anomaly signals were reduced to pole thereby minimizing polarity effects on the data by setting the inclination (I) and declination (D) angles at −24.78° and 0.45° respectively in Eq. (3) (Durrheim and Cooper,1998; Omenikolo, Emberga, and Opara, 2022; Bahi, 2024), thus transforming the magnetic signal amplitude $A(f)$ at a frequency f into its filtered version $A'(f)$ for vertical inclination.

$$A'(f) = \frac{A(f)}{\left(\sin(I) + \sqrt{-1}\cos(I)\sin(D)\right)^2} \tag{3}$$

The reduced-to-pole signal is then subjected to Centre of Exploration Targeting (CET) processing to enhance, locate, and vectorize discontinuities using a series of algorithms on magnetic data. CET performs grid texture analysis and bilateral symmetric feature detection, giving reliable trend detection for large data sets (Holden et al.,

2012; Tsepav, 2020; Trepil et al., 2021). Windowing initiates the texture analysis process by the application of a standard deviation filter that produces high standard deviation values at the regions of discontinuity (Holden et al., 2012). The local texture is characterized using image entropy (E) to measure the trends of pixel intensities within the local neighborhood. The entropy calculation can be performed using Eq. (4) on a given bin i of n number of bins with p_i histogram value (Holden et al., 2010). A window size of 7 for a ratio of 1:87 m was used.

$$E = -\sum_{i=1}^{n}(p_i \log(p_i)) \tag{4}$$

To examine the signal frequency components using Fourier analysis, phase symmetry was determined by setting the filter scale number at 3 and symmetry robustness at 1 for all orientation angles. The line segments obtained were then vectorized at a thresholding value of 0.1 within 2 cells. The vectorized line segments were subjected to an iterative morphological operation that allowed the thinning of the objects to about 1-pixel width. The resultant lineaments were assigned coordinates, mapped, and the corresponding rose diagram drawn.

3.4 Lineament Characterization

Lineaments A to Z had cross-sectional slices 1 to 7 cut across them to map the depths and orientations of the possible structures (Fig. 4). The slices targeted the structures mapped from the residual magnetic grid.

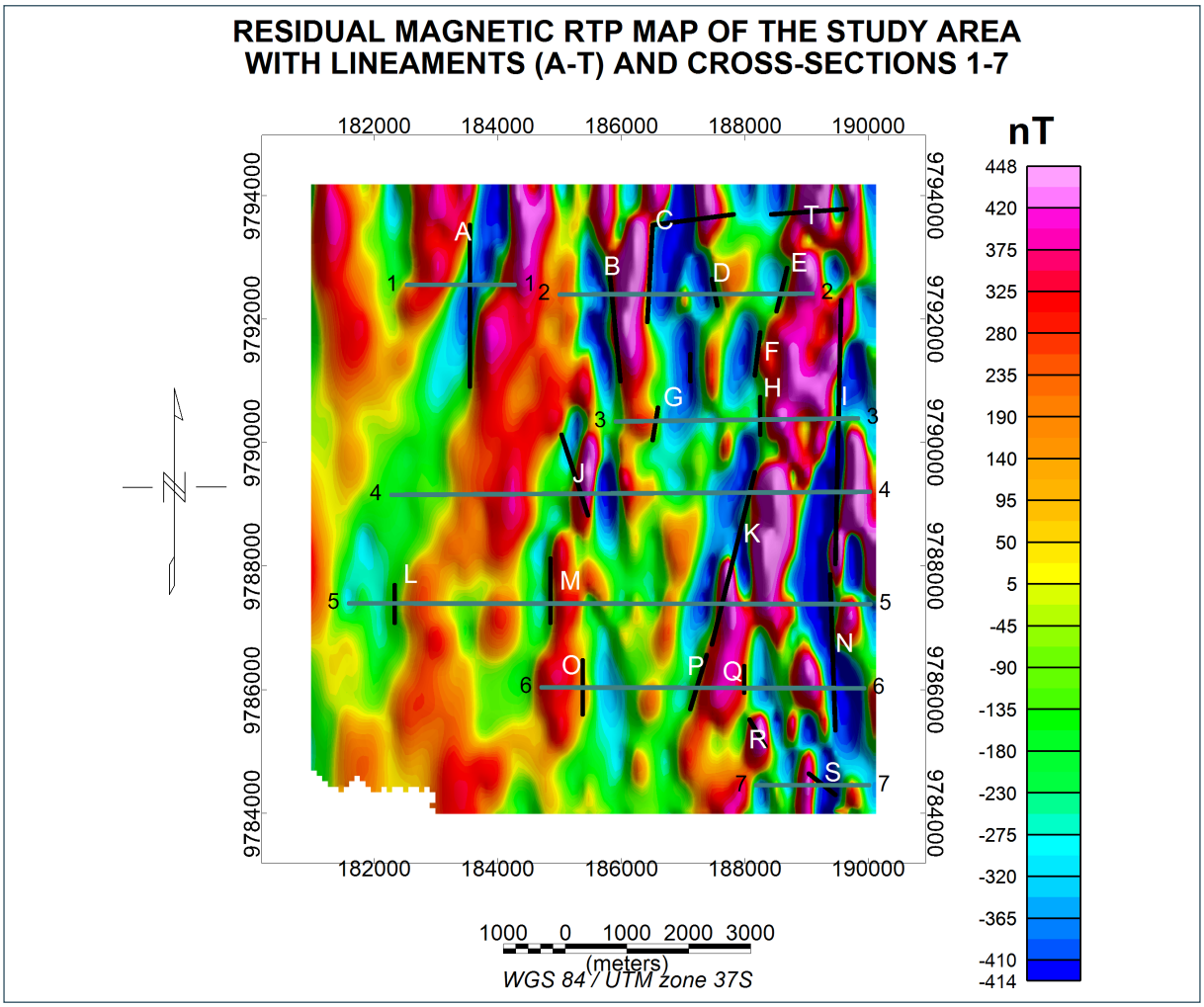

Figure 4. RTP Residual Magnetic Anomaly Map with Lineaments A-T and Cross-section slices 1-7.

The slice data were then subjected to 2D Euler deconvolution based on the standard Euler equation (Eq. (5)) to obtain solutions on structures of interest. Structural Indices (N) of 0 to 1, which are ideal for solution clustering along faults or tectonic boundaries, were tested on the magnetic data (Durrheim and Cooper, 1998; Minelli et al., 2016; Olafisoye, Adegoke, and Alagbe, 2022; Cooper, 2024, Deep, 2024). A correct choice of N produces Euler solutions that cluster tightly along/around the geologic structure of interest (Olafisoye, Adegoke, and Alagbe, 2022).

$$(x - x_0)\frac{\partial F}{\partial x} + (y - y_0)\frac{\partial F}{\partial y} + (z - z_0)\frac{\partial F}{\partial z} = N(B - F) \tag{5}$$

The values of x_0, y_0, z_0 form the coordinates of the magnetic anomaly source whose total field intensity F, and regional value B were measured at the point defined by x, y, z. A window size of 10 was used throughout. A total of 7 Euler plots were obtained and analyzed to characterize lineaments.

4. Results and Discussion

The residual magnetic anomaly map of the study area (Fig. 5) used to characterize faults from lineaments shows a high population of detected magnetic sources along the eastern zone of the study area. The map can also be used to detect volcanic intrusions, faults, fractures, lithological boundaries, and buried structures. Yellow to pink shades represent high magnetic regions, while purple to blue shades represent low magnetic regions. The presence of the closed magnetic anomalies in the regions neighboring Lake Magadi (between 186000E and 190000E) provided a critical geological insight into the location of magmatic intrusions. A comparison with the reduced-to-pole

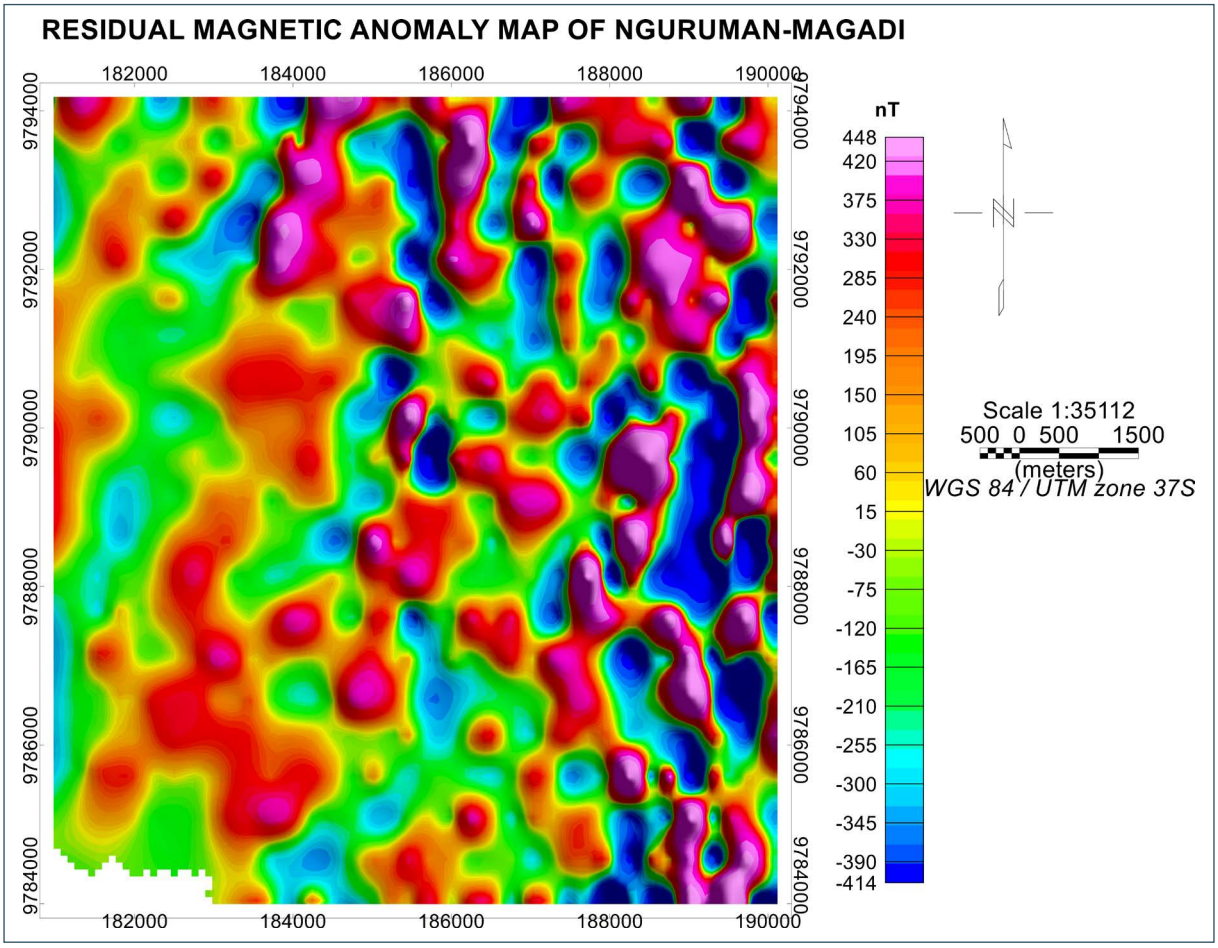

Figure 5. Residual Magnetic Anomaly map of the Study area.

magnetic map (Fig. 4) presents high magnetic anomalies (>375 nT) to the east of the study area, where the trachytic formations are dominant. The high zones can be associated with the remnants of rift-related mafic volcanism, such as Pleistocene Magadi trachyte and shallow Plio-Miocene Olivine Basalts forming the magnetic basement. They may also indicate dykes or sills associated with early rifting in the area. The widespread trachytes and the dominant magnetic anomalies in the eastern zone are indicators of cooling magmatic intrusions.

Figure 5 reveals relatively low-level magnetization in the western zones of the study area. The low magnetic anomalies (<−200 nT) can be linked to the sedimentary basins or fault-bounded troughs where Holocene sediments such as alluvial terraces and the widespread lacustrine deposits have accumulated. The thick sedimentary cover of the Pleistocene Oloronga lake beds and the heavily altered or weathered volcanic rocks in the central and western regions (Fig. 2) have contributed to the reduced magnetic intensities (Pratama et al., 2018; Srivastava et al., 2023).

Zones with abrupt color changes suggest major structural discontinuities such as contacts between lithological units, faults, fractures, and dyke swarms. The patterns are consistent with the structural features shown in the geological map (Fig. 2) and the reports from previous investigations showing the N-S structural trends (Komolafe et al., 2012). These structures control the location of hot springs by enabling geothermal fluid flow (Komolafe et al., 2013). Figure 5 presents the Magadi-Nguruman area as a tectonically active rift zone with geothermal potentials and volcanic centers towards the east of the study area.

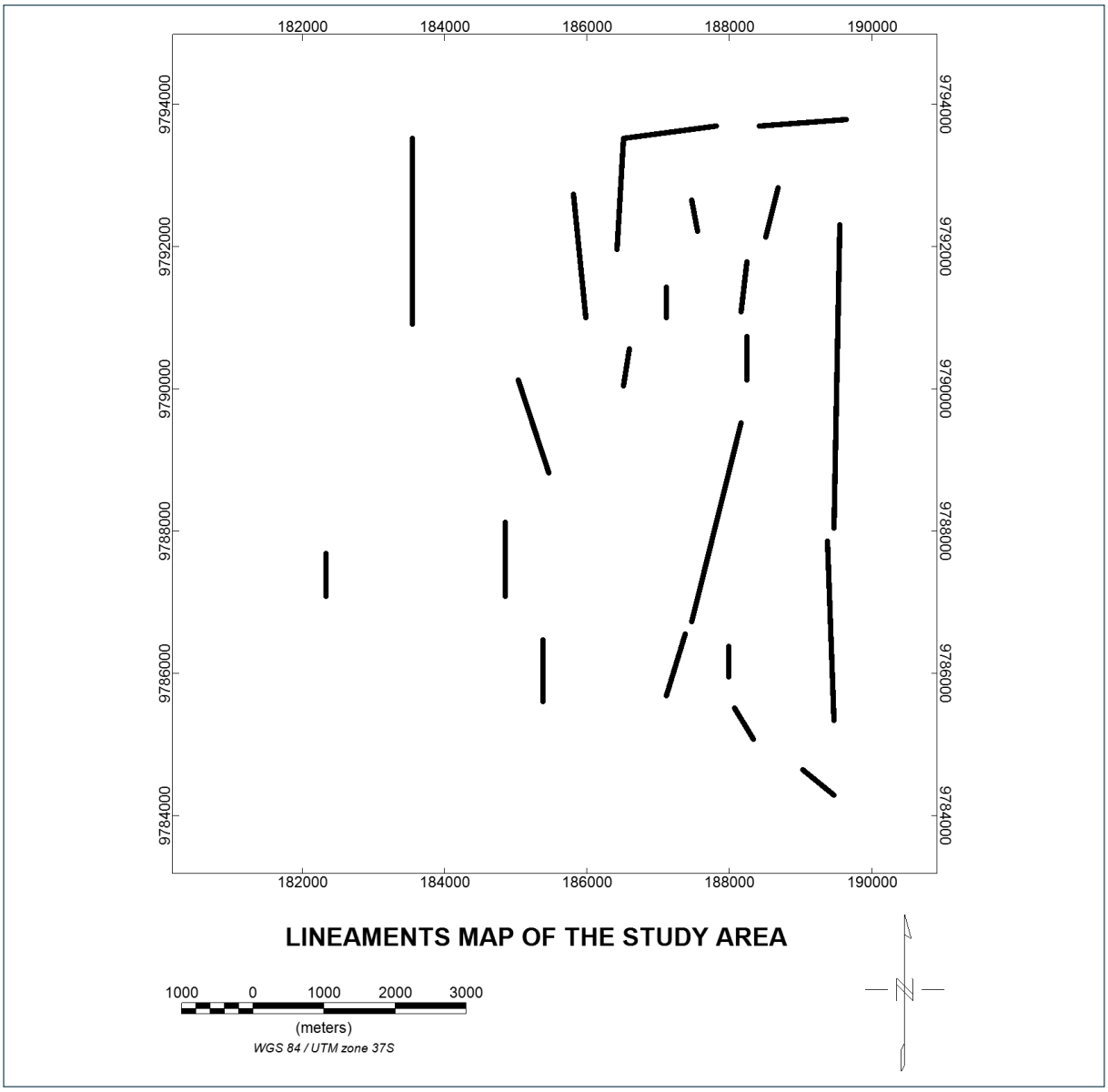

Figure 6. Distribution Map of the Lineaments over the study area.

Figure 6 located the majority of the lineaments to the east of the study area, close to active hot springs, heated Lake Magadi, and exposed faults. The high temperature of the springs and the lake can be linked to the heat from magmatic intrusions. Other studies involving gravity mapping over the area associate high gravity anomalies and heat flux patterns from intrusive heat sources with possible geothermal potentials (Nyakundi et al., 2021; Odero et al., 2024).

The lineaments trace major faults, minor faults, joints, lithological contacts, shear zones, and troughs or ridges. They reveal underlying rock architecture that can describe a geothermal system together with water recharge mechanisms (Altinoğlu, 2023; Çelik, 2019). The hydrothermal system of regions within and around Lake Magadi is dependent on underground hot water inflow and recharge from surface waters (Komolafe et al., 2012). The recharge is made possible mainly through faults and fractures. This study presents an additional method for fault characterization from lineaments using CET on magnetic data to improve the process of mapping thermal structures in a geothermal potential zone such as Magadi. Discussions on the tectonic activities in Magadi delineate young fault scarplets, neotectonic extension joints, and magmatic intrusions as structurally consistent with the lineament patterns in Fig. 6 (Behr and Röhricht, 2000; Muirhead et al., 2016). Kodikara et al. (2016) emphasize the correlation between mineral deposition patterns in Magadi and the underlying geological and hydrothermal structures within the sedimentary layers.

An overlay of lineaments on the RTP magnetic anomaly map shows a significant relationship between the distribution of magnetic anomalies and the lineaments (Fig. 7). The most extensive lineaments are found within the

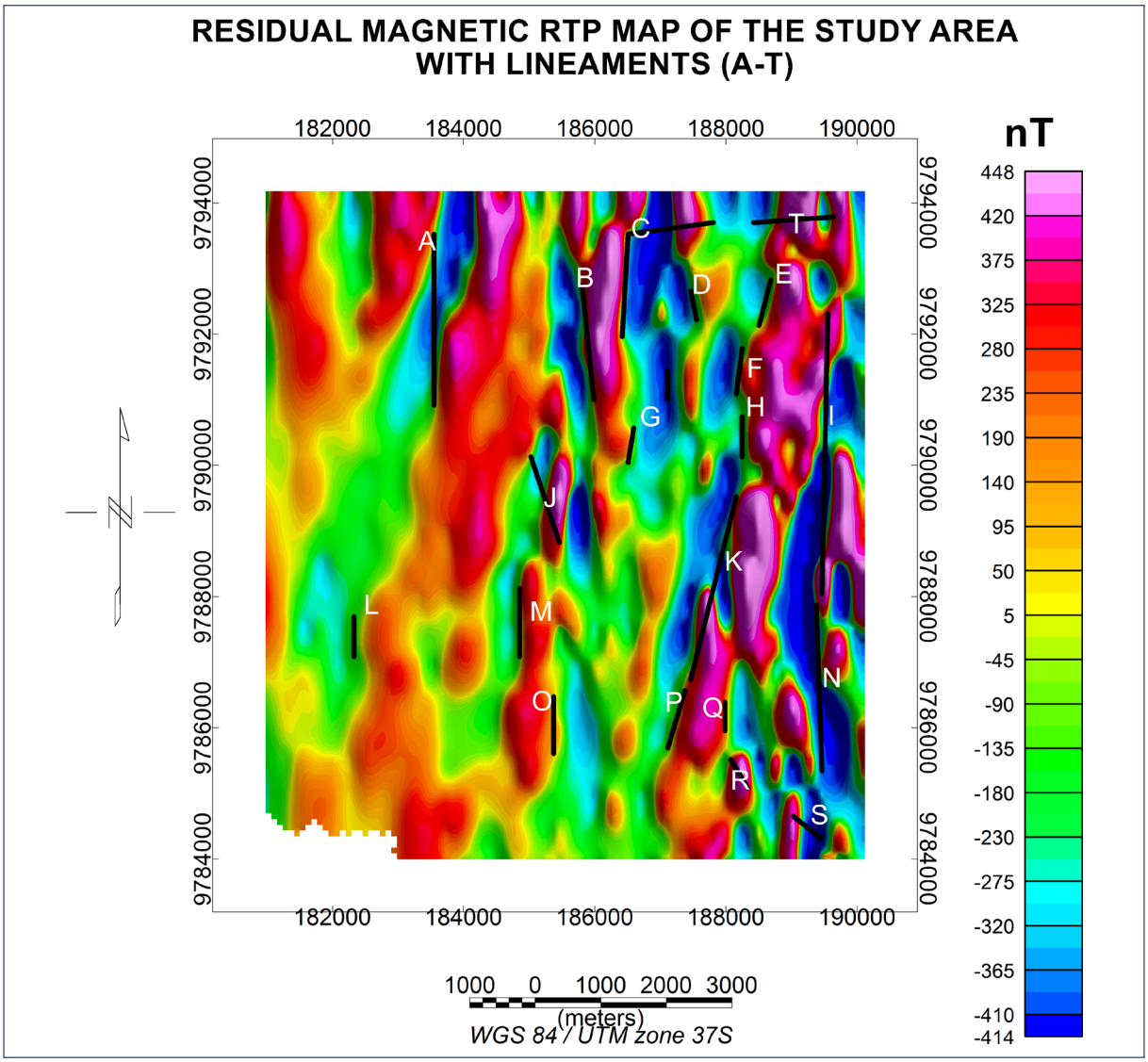

Figure 7. Residual Magnetic Anomaly Map with Lineaments overlay.

anomalous eastern zone of the study area, indicating strong tectonic events in the area throughout geologic history. The general orientation of the lineaments, as shown by the rose diagram, is in the N-S direction (Fig. 8). Figure 8 displays that the NE-SW trending lineaments are dominant. They could represent normal faults parallel to the main rift trend, boundary faults controlling the main graben structure, or zones where magnetic anomalies shift. The result coincides with the geologically reported orientation of faults, rift escarpments, hot springs, and travertine belts in the area (Gloaguen et al., 2007; Muirhead et al., 2016; Zou et al., 2023). The second dominant set of lineaments are NW-SE trending. They could be a representation of transfer faults, oblique-slip faults, or pre-rift basement fractures reactivated during rifting (Chorowicz, 2005; Sequar, 2009), showing structural control on basin formation. The N-S trending lineaments infer possible fracture zones influencing modern hydrothermal systems. Where the N-S and the NE-SW faults intersect could be zones of enhanced permeability necessary for geothermal reservoirs (Vignaroli et al., 2013; Wiyono et al., 2022). High-density lineaments correspond to structural complexity (Ghalati et al., 2023). High structural complexity with high magnetic relief represents possible opportunities for exploring magmatic heat sources.

The analysis of data from the cross-sectional slices 1 to 7 using the Euler deconvolution approach (Eq. (5)) aided in the detection of faults. 2 D Euler inversion process gives solutions that correspond approximately to the top of the magnetic sources (Komolafe et al., 2012). The alignment and scattering of the Euler solutions reveal the geometry of the underlying tectonic structures (Williams et al., 2005; Komolafe et al., 2012). The accuracy of the inversion results is largely dependent on the right selection of structural indices corresponding to the geologically presumed source body (Olafisoye, Adegoke, and Alagbe, 2022). The ability to ascertain the spatial orientation of geological structures through Euler deconvolution is paramount in a tectonically active area like Magadi, where fault systems and heat sources critically interface with hydrothermal features.

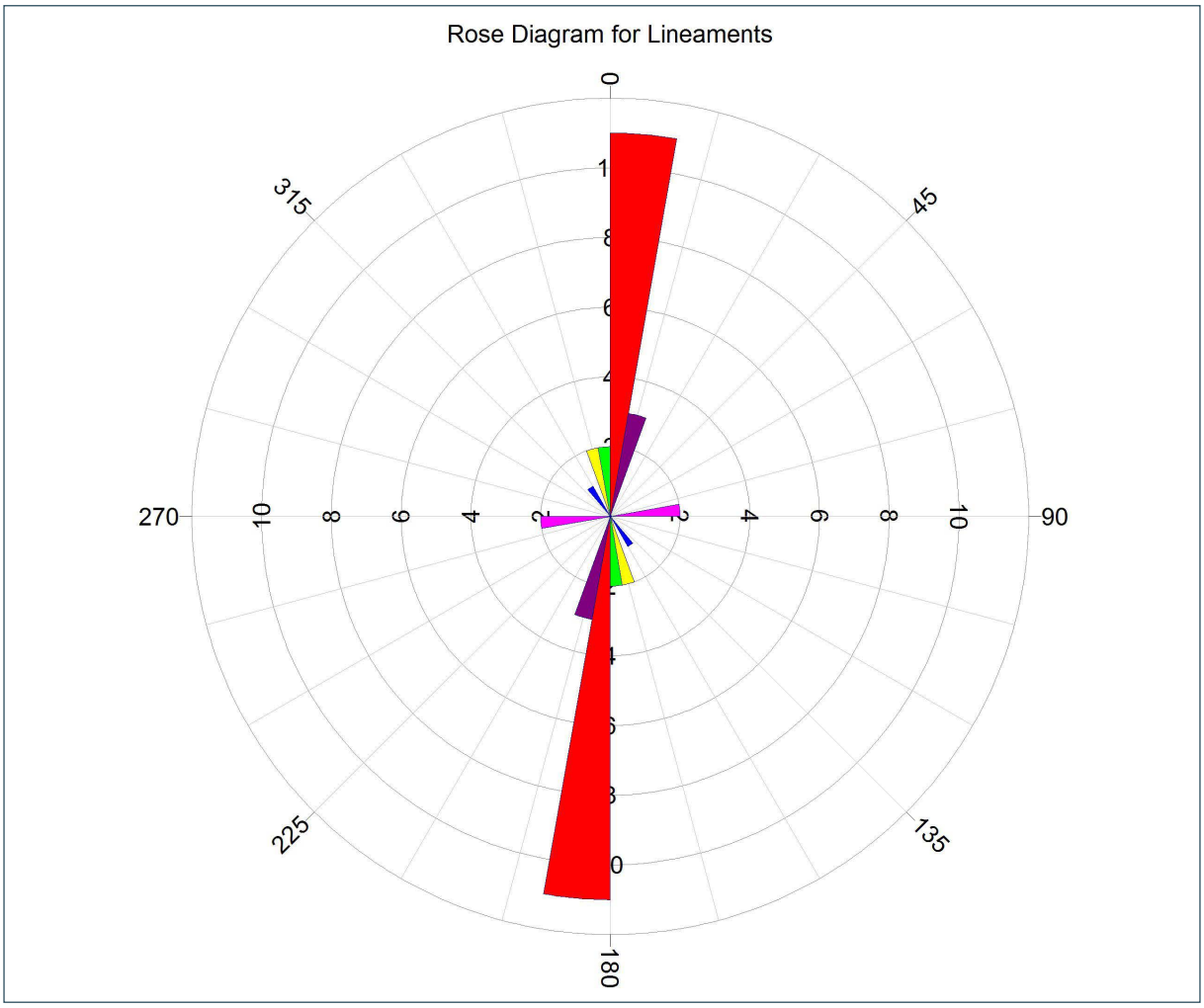

Figure 8. Rose Diagram showing the Lineament Orientations.

Euler solutions from slice 1 delineated an inter-layer contact with a varying depth (240 m to 270 m). The horizontal layer, which can be interpreted to be the interface between the lower Holocene sedimentary formation and the Basaltic basement, showed no relationship with lineament A, implying that lineament A is neither a fault nor a vertical contact (Fig. 9). Previous studies indicate that the depth of the Holocene sediments in the western regions of Lake Magadi is dynamic as a result of changing climatic and volcanic cycles (Owen et al., 2018; Behr and Röhricht, 2000), an observation which is consistent with the depth patterns revealed by the solutions in Fig. 9. Figure 10 provides Euler solutions and anomaly trends over lineaments B, C, D, and E. Lineament C missed the Euler detection, while lineaments B, D, and E manifested as faulted contacts. Cross-sectional slice 3 mapped out lineaments H and I but failed to show the fault attributes of lineament G (Fig. 11). The Euler solutions for slice 4, aimed at characterizing lineaments J, K, and I (Fig. 12), turned positive for fault analysis.

Similarly, the faults responsible for lineaments L, M, K, and N were successfully detected using the calculated solutions from data obtained from cross-sectional slice 5 as depicted in Fig. 13. Figures 14 and 15 are plots of cross-sectional slices 6 and 7 respectively. The plots indicate the solutions for the subsurface detection of faults linked to the lineaments O, P, Q, N, and S.

Table 1 summarizes lineament characteristics in terms of orientation, detection, identity, strike, dip angle, and approximate depth. The table shows an approximate depth range of 240 m to 740 m. The location of the deeper faults close to observable hot springs agrees with the characteristics of the five major faults delineated by Komolafe et al. (2012). Considering the continuous effects of fluids released from magmatic sources on fault lines and fault interactions, resulting in an approximate slip rate of 0.42-0.7 millimeters per year (Muirhead et al., 2016), the reported depths are consistent with the results in Table 1 (Shet et al., 2001). The dip angles range from 32° to 83° for all 16 detected faults. Two lineaments, A and G, were identified as troughs while two others, C and T, as ridges based on the correlation of Euler deconvolution and observed geology of the study area. A map of characterized lineaments is shown in Fig. 16, clearly indicating the strike and dip directions of the detected faults. The general N-S orientation of the detected faults and the dipping directions towards the basement of Lake Magadi to the south are important facts to consider when mapping the possible geothermal system at Magadi.

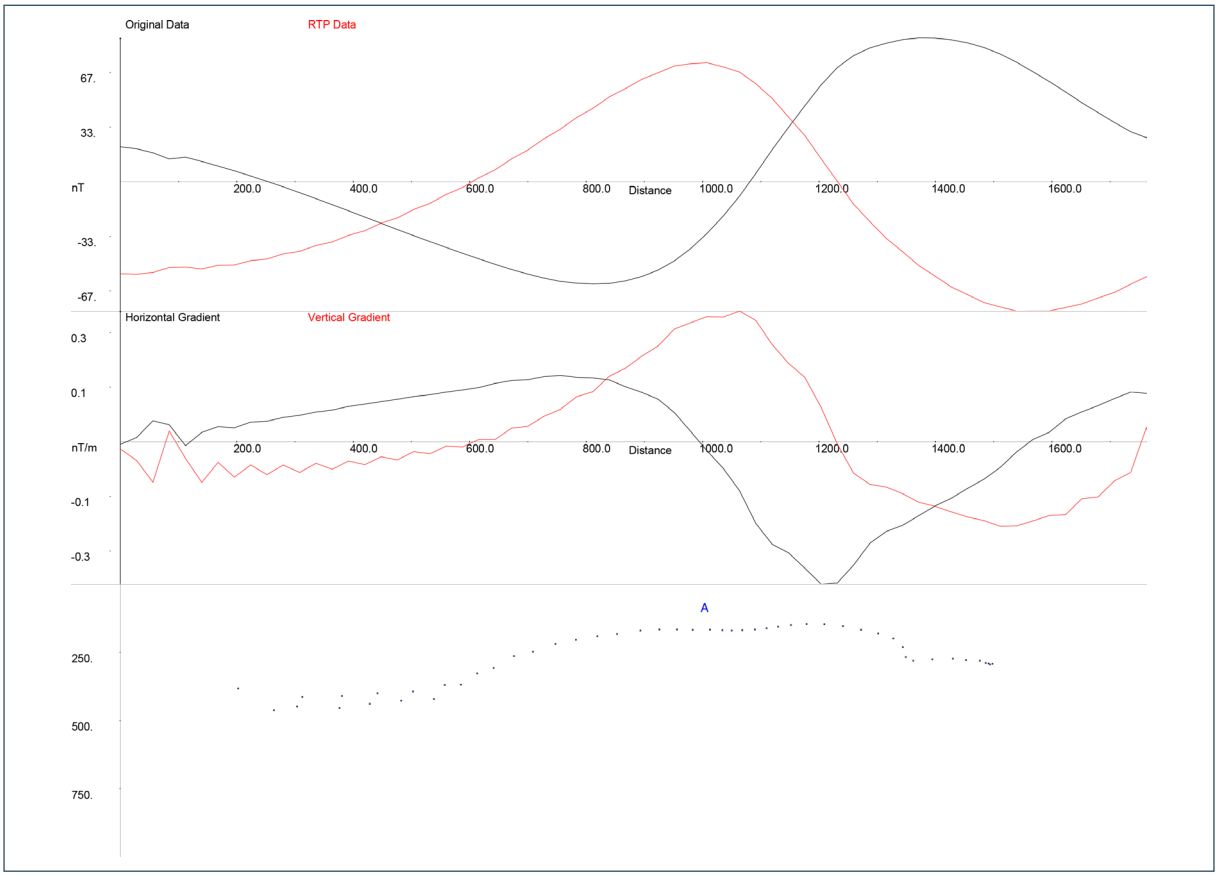

Figure 9. Euler Solutions for Cross-section slice 1 over Lineaments A.

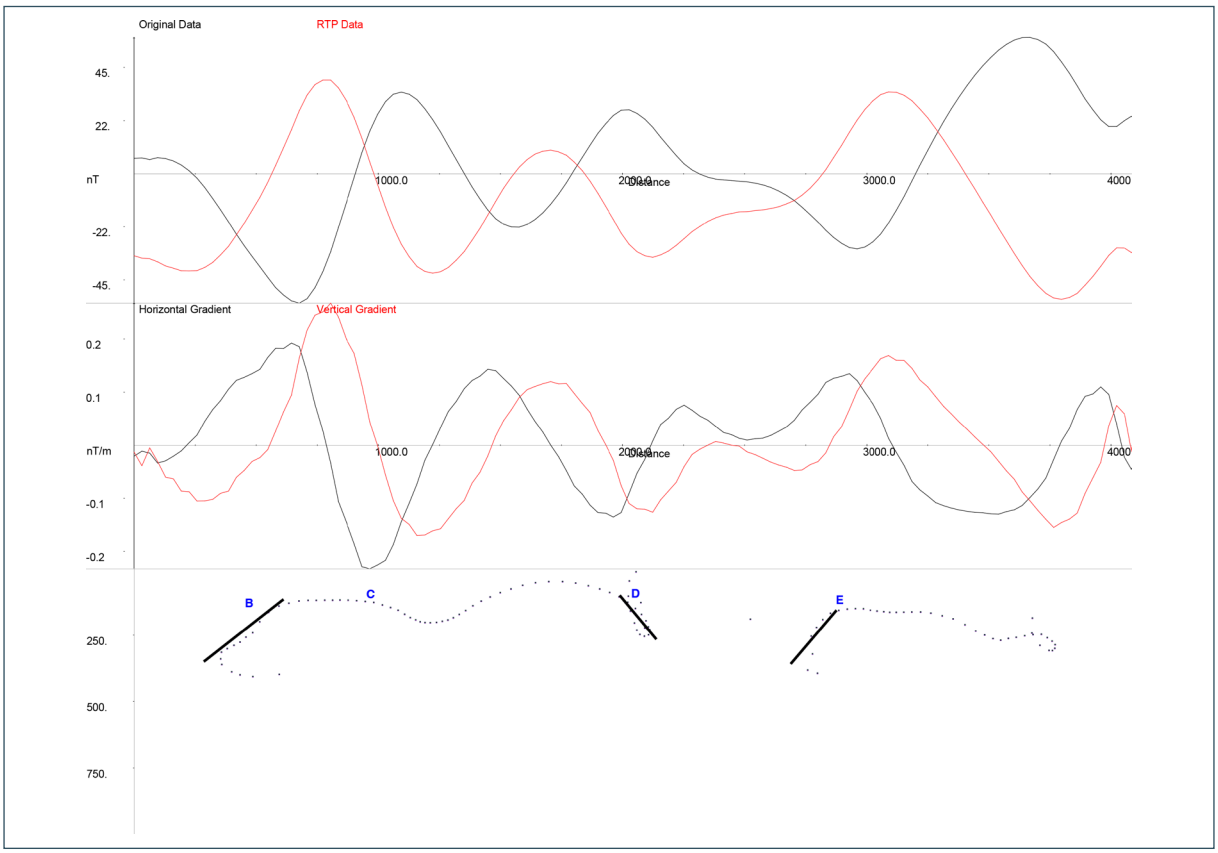

Figure 10. Euler Solutions for Cross-section slice 2 over Lineaments B, C, D, and E.

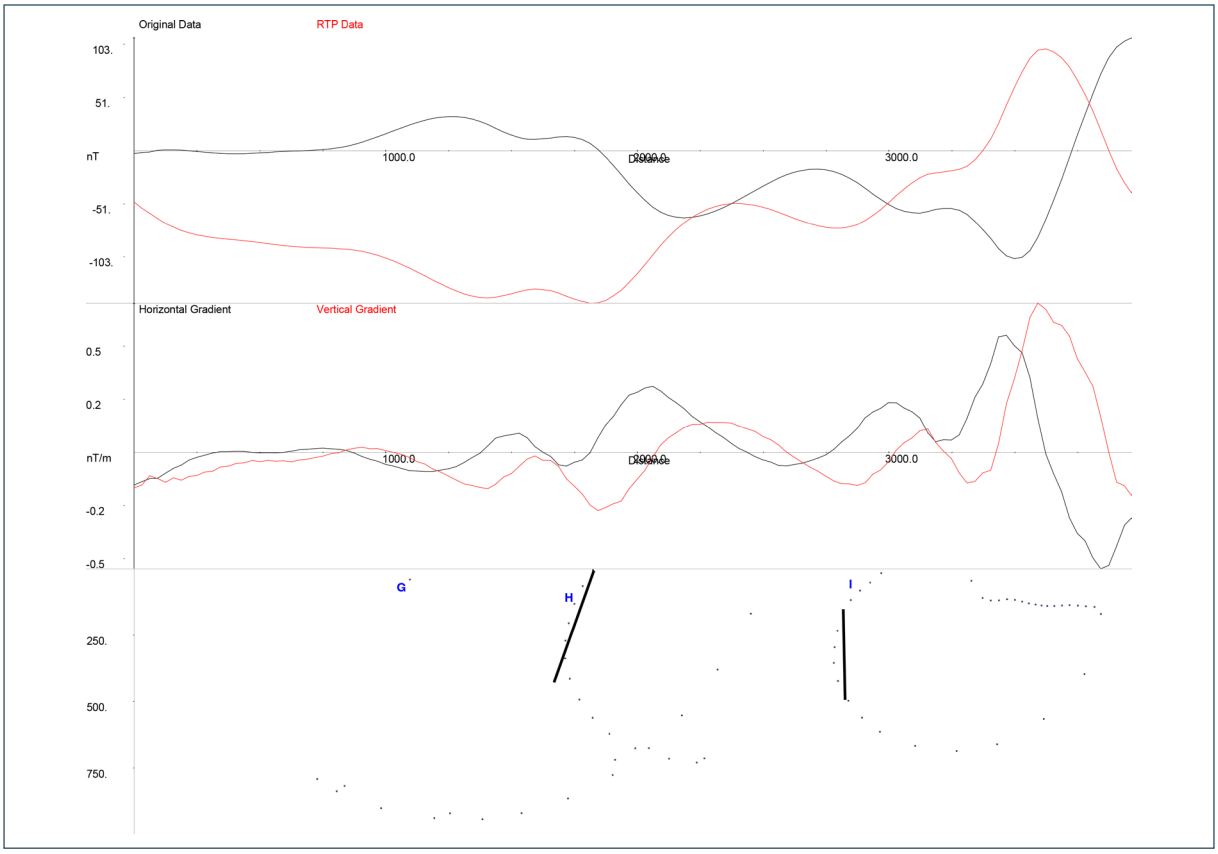

Figure 11. Euler Solutions for Cross-section slice 3 over Lineaments G, H, and I.

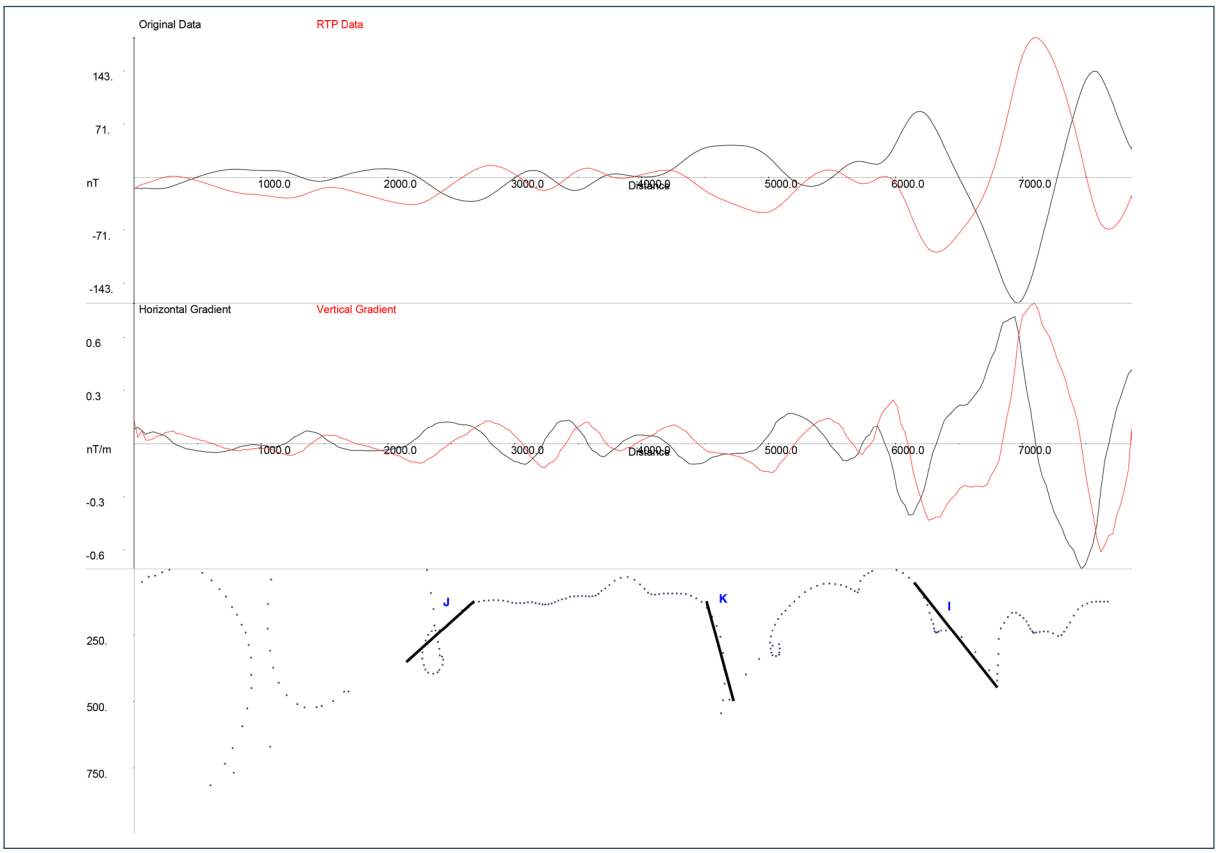

Figure 12. Euler Solutions for Cross-section slice 4 over Lineaments J, K, and I.

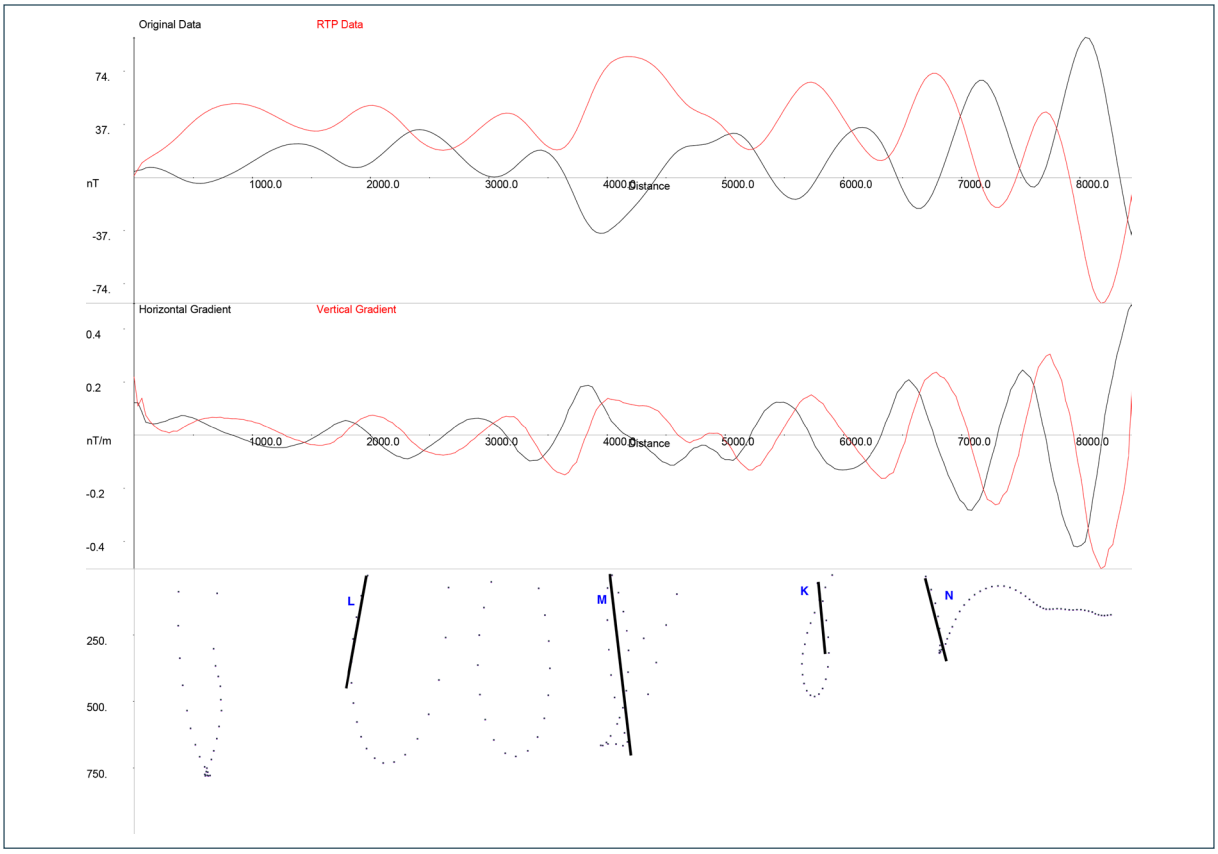

Figure 13. Euler Solutions for Cross-section slice 5 over Lineaments L, M, K, and N.

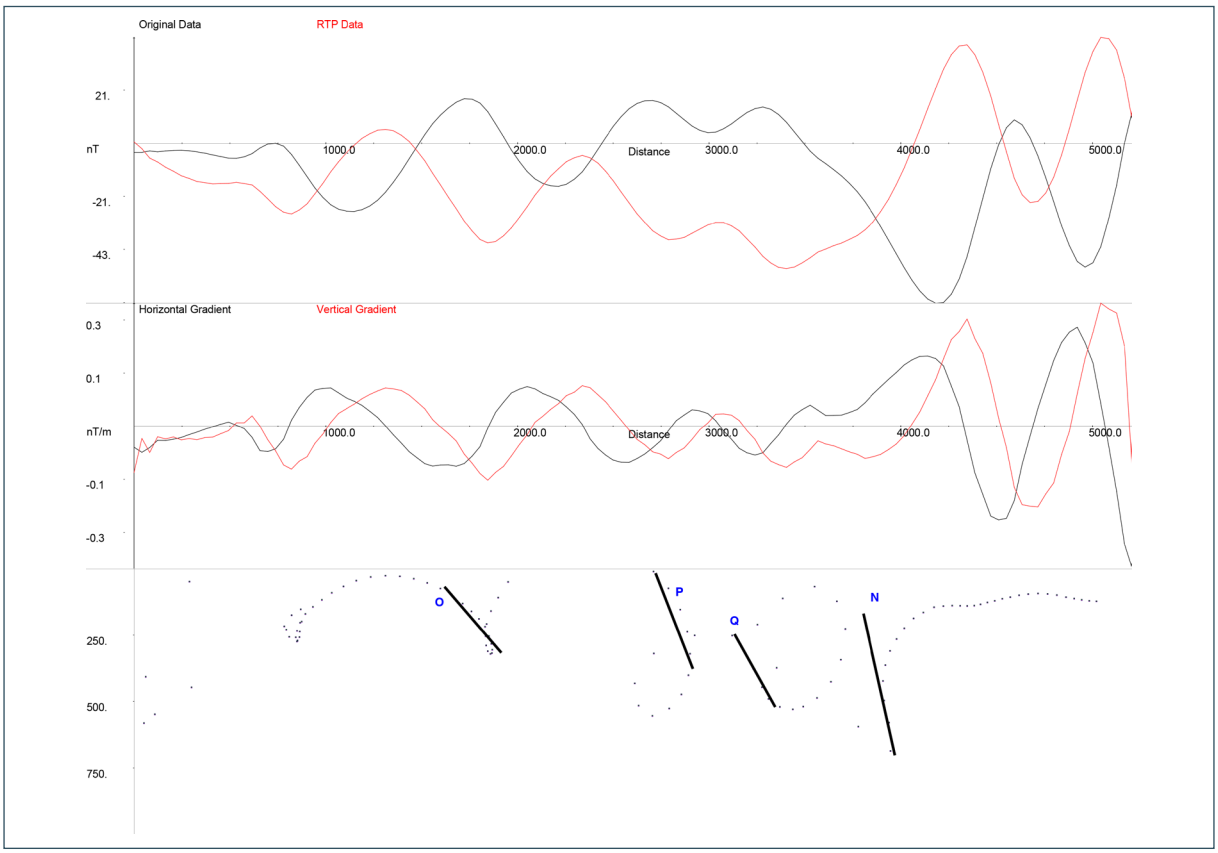

Figure 14. Euler Solutions for Cross-section slice 6 over Lineaments O, P, Q, and N.

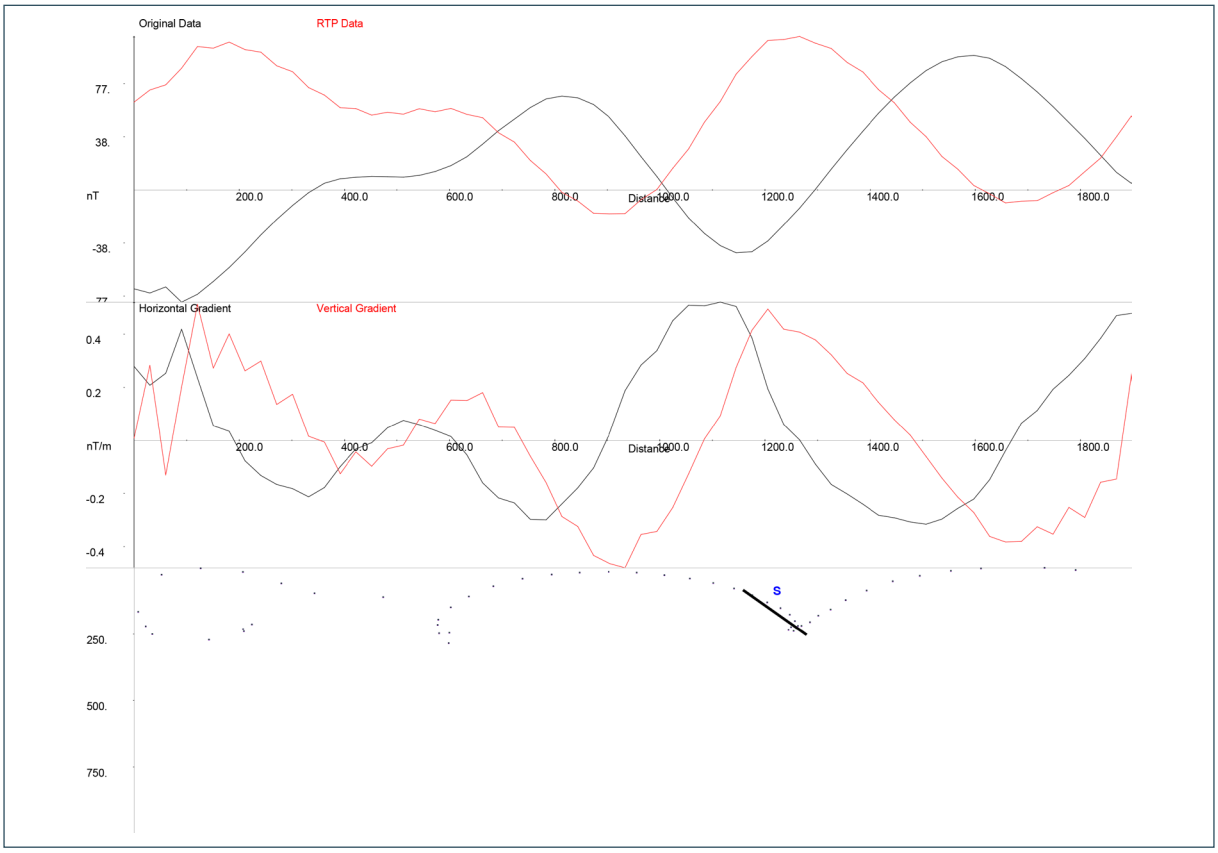

Figure 15. Euler Solutions for Cross-section slice 7 over Lineament S.

Table 1. Lineament Characteristics.

Lineament	Orientation	Detection	Identity	Strike	Dip (Deg.)	Depth (m) (Approx.)
A	N-S	–	Trough			
B	NNW-SSE	+	Fault	S07°E	36.45°	400
C	N-S	–	Ridge			
D	NNW-SSE	+	Fault	S15°E	49.41°	250
E	NNE-SSW	+	Fault	S17°W	49.93°	410
F	N-S	+	Fault	N-S	59.67°	435
G	NNE-SSW	–	Trough			
H	N-S	+	Fault	N-S	69.4°	460
I	N-S	+	Fault	N-S	51.02°	480
J	NNW-SSE	+	Fault	S20°E	39.41°	350
K	NNE-SSW	+	Fault	S14°W	74.20	500
L	N-S	+	Fault	N-S	79.25°	420
M	N-S	+	Fault	N-S	82.86°	740
N	N-S	+	Fault	N-S	74.1°	730
O	N-S	+	Fault	N-S	49.74°	300
P	NNE-SSW	+	Fault	S15°W	67.92°	360
Q	N-S	+	Fault	N-S	59.51°	500
R	NNW-SSE	+	Fault	S36°E	48.1°	370
S	NW-SE	+	Fault	S50°E	36.68°	240
T	W-E	–	Ridge			

The protocol for fault characterization from lineaments, based on magnetic data, has been summarized in Fig. 17. The components of the chart have been discussed in various sections of this work. The protocol presents a reduced-to-pole total magnetic intensity (TMI) map as a crucial input to the lineament generation process. The CET processes include windowing, lineation, vectorization, skeletonization, and coordinate determination. The mapped lineaments inform the orientations of Euler cross-sections. It is the relationship between the patterns of Euler

solutions and the location of the corresponding lineaments that informs the lineament characterization as either fault, ridge, or trough. The greatest strength of the protocol lies in its ability to identify and characterize fault-linked lineaments using anomalies in a potential field, to produce an informative map akin to what Fig. 16 presents.

From the rose diagram analysis, orientation characteristics can be obtained to show the directions of alignment of the majority of lineaments. The dominant lineament trends are geologically significant in structural control mapping. The number of lineaments in a given direction can be determined from the petal lengths. Symmetric rose patterns can reveal systemic or tectonic origins, while asymmetric patterns speak to localized structural influences.

Detection, identity, strike, dip and approximate depth in meters can be deduced from the analysis of Euler solutions. The application of the protocol to the data obtained from Magadi resulted into the characteristics tabled in Table 1. Majority of the long faults were located in the east and central regions of the study area, indicating higher

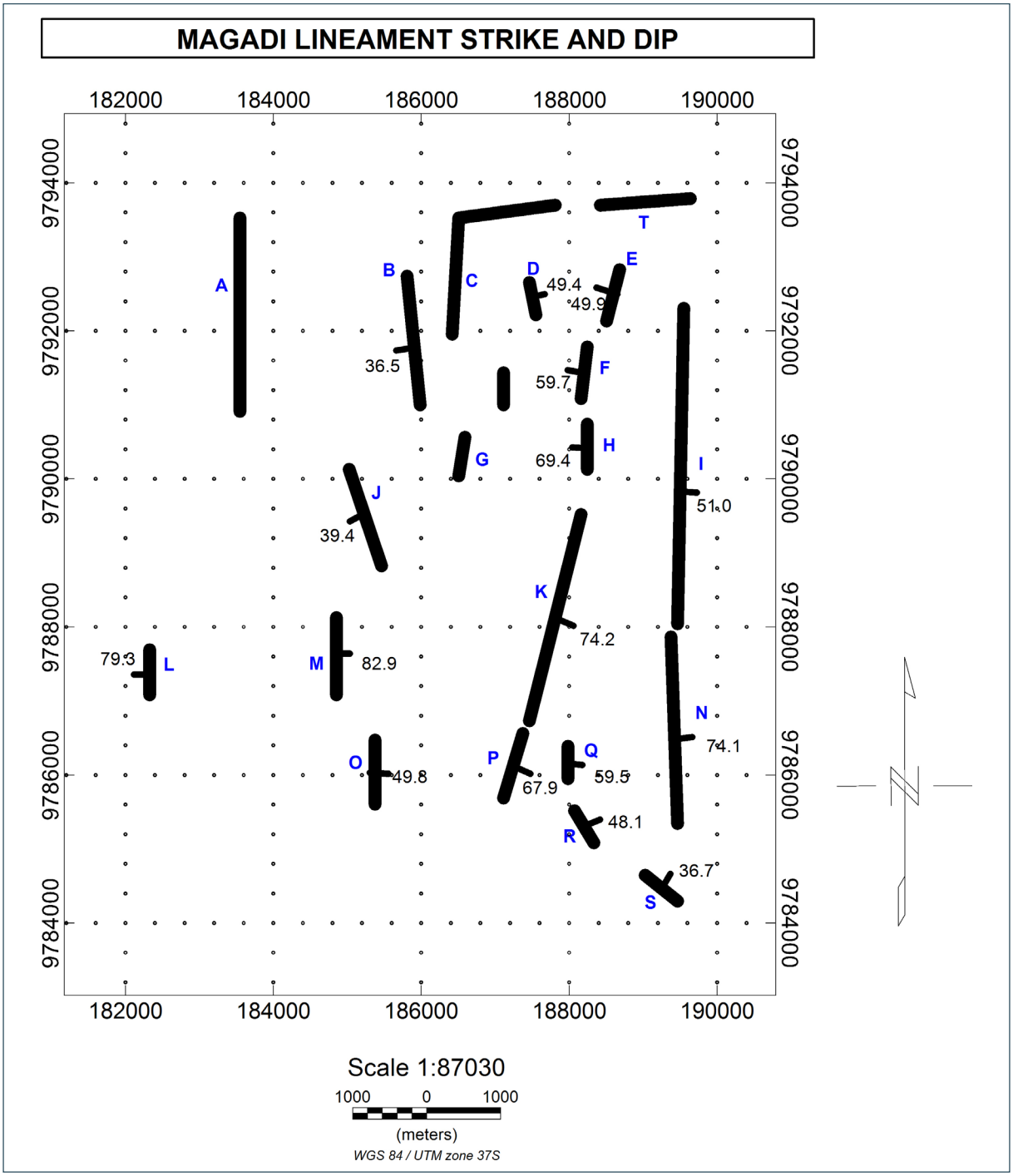

Figure 16. A map of characterized lineaments in the Magadi-Ngurumann Area.

permeability of subsurface formations. Faults closer to lake Magadi were found to dip towards the bottom of the lake and the areas with active hot springs. The west of the study area was least populated by the detected faults, showing reduced tectonic activities in the area dominated by lacustine sediments.

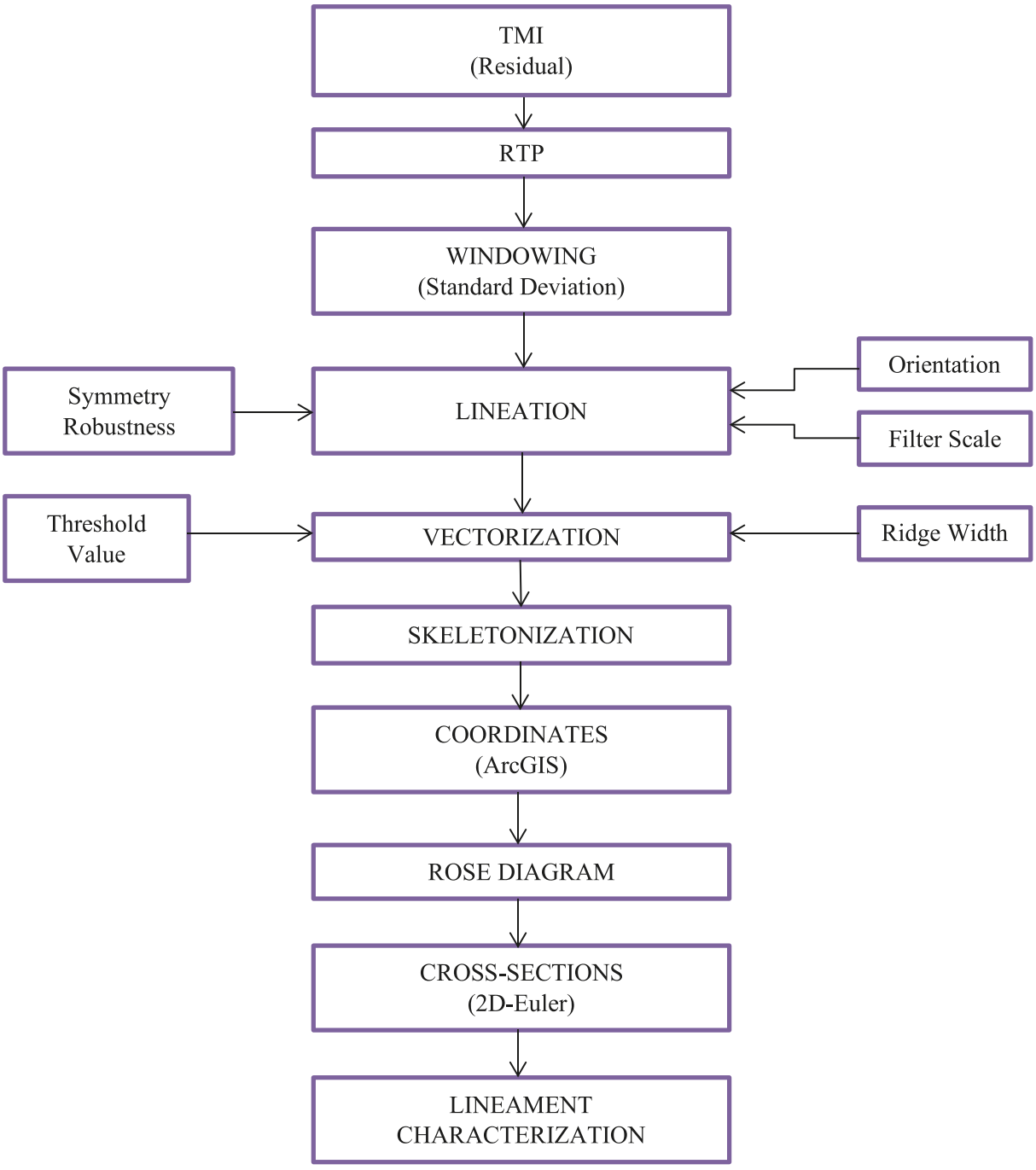

Figure 17. Lineament Characterization Protocol based on Magnetic Data Map.

5. Conclusions

Fault characterization from lineaments based on magnetic data has been performed, and the protocol has been produced. The study provides a reliable procedure for fault characterization from lineaments based on magnetic data. The procedure involved the CET processes and Euler Deconvolution. When applied to the magnetic data of the Magadi-Nguruman area with high magnetic anomalies (>375 nT) to the east of the study area, where the trachytic

formations are dominant, the results show that the study area is sufficiently faulted for a possible geothermal system near Lake Magadi. 80% of the lineaments were characterized as faults. 81.25% of the detected faults strike in the near N-S direction, which is in harmony with the geological description of the structural trends in the region. The dipping angles of the detected faults range between 36.45 and 82.86 degrees. 62.5% of the faults dip towards the basement of L. Magadi, thereby showing a possible relationship between the tectonic structures and magmatic movements. The detected faults extend to depths ranging from 0.25 km to 0.74 km, which can be considered sufficient for proper transmissivity to subsurface reservoirs. The deepest structures were located within a 3 km stretch from the edge of Lake Magadi.

Data availability statement. The data used in this study can be accessed from the departmental repositories of the Department of Physics at Jomo Kenyatta University of Agriculture and Technology upon request.

Acknowledgements. Special thanks to the African Development Bank for collaborating with the Jomo Kenyatta University of Agriculture and Technology to fund this research. I'm greatly indebted to the National Oil Corporation of Kenya for software support. Much gratitude goes to the Ministry of Geology and Mines for availing the geological report for the study area. I dearly recognize the supervisory support from the Department of Physics at the Jomo Kenyatta University of Agriculture and Technology.

References

Abdullah, A., R. Puspita and H. Hamad (2020). Review of Regional Geological Structures on the appearance of Geothermal Manifestations in the "neck" region of western Sulawesi Island, Matec. Web. Conf., 331, 03003, doi:10.1051/matecconf/202033103003.

Ahmadi, H. and E. Pekkan (2021). Fault-based Geological Lineaments Extraction using Remote Sensing and GIS – a review, Geosci., 11, 5, 183, doi:10.3390/geosciences11050183.

Alexander, K. B., G. Ussher and S. K. Merz (2011). Geothermal Resource Assessment for Mt Longonot, Central Rift Valley, Kenya, in Proceedings of the GRC Annual Meeting, San Diego, CA, USA, 23-26.

Altinoğlu, F. F. (2023). Mapping of the Structural Lineaments and Sedimentary Basement relief using Gravity data to guide Mineral Exploration in the Denizli Basin, Minerals Basel, 13, 10, 1276, doi:10.3390/min13101276.

Atmaoui, N. and D. Hollnack (2003). Neotectonics and the Extension Direction of the Southern Kenya Rift, Lake Magadi area, Tectonophysics, 364, 1-2, 71-83, doi:10.1016/s0040-1951(03)00051-9.

Bahi, A., Y. Zerradi, M. Bziaz, Y. Tlidi et al. (2024). Characterization of Mineral Deposits using the Magnetic method: the case of the Aïn Beida Mine in Bouarfa, Morocco, Civ. Environ. Eng., 20, 1, 571-579, doi:10.2478/cee-2024-0043.

Bauernhofer, A., C. Hauzenberger, E. Wallbrecher, G. Hoinkes et al. (2000). Strain and Kinematic Analysis of major Tectonostratigraphic Units from the Mozambique Belt of the Voi district, Southeast Kenya and the Pare-Usambara Mountains, Northeast Tanzania, J. Afr. Earth Sci., 30, 4A, 10, doi:10.1007/s00531-008-0345-9.

Behr, H. and C. Röhricht (2000). Record of Seismotectonic Events in Siliceous Cyanobacterial Sediments (Magadi Cherts), Lake Magadi, Kenya, Int. J. Earth Sci., 89, 2, 268-283, doi:10.1007/s005319900070.

Çelik, R. (2019). Evaluation of Groundwater Potential by GIS-based Multicriteria Decision Making as a Spatial Prediction Tool: Case Study in the Tigris River Batman-Hasankeyf Sub-Basin, Turkey, Water-Sui, 11, 12, 2630, doi:10.3390/w11122630.

Çetintaş, S. (2022). Investigation of Pore and Filling Material Bond in filled Travertine used as a Building Material, Period. Polytech. Civ., doi:10.3311/ppci.20845.

Choi, W., S. Cho, D. Inoue, M. Yanagida et al. (2016). Lineament Analysis using ASTER Satellite Images in the Southern part of the Korean Peninsula, J. Georeng., 4, 1, doi:10.17265/2328-2193/2015.01.002.

Chorowicz, J. (2005). The East African Rift System, J. Afr. Earth Sci., 43, 1-3, 379-410, doi:10.1016/j.jafrearsci.2005.07.019.

Cooper, G. R. J. (2024). Using Euler Deconvolution as part of a Mineral Exploration Project, Minerals Basel, 14, 4, 393, doi:10.3390/min14040393.

Durrheim, R. J. and G. R. J. Cooper (1998). Euler Deconvolution of Magnetic and Gravity Data, Comput. Geosci., 24, 7, 545-550, doi:10.1016/s0098-3004(98)00022-3.

Gentana, D., N. Sulaksana, E. Sukiyah and E. Yuningsih (2019). Morphotectonics of the Mount Rendingan area related to the appearances of Geothermal Surface Manifestations, Indones. J. Geosci. 6, 3, 291-309, doi:10.17014/ijog.6.3.291-309.

Getenet, M., J. M. García-Ruiz, C. Verdugo-Escamilla and I. Guerra. (2020). Mineral Vesicles and Chemical Gardens from Carbonate-rich Alkaline Brines of Lake Magadi, Kenya, Crystals, 10, 6, 467, doi:10.3390/cryst10060467.

Ghalati, F. H., J. A. Craven, D. Motazedian, S. E. Grasby et al. (2023). Analysis of Fluid Flow Pathways in the Mount Meager Volcanic Complex, Southwestern Canada, utilizing AMT and Petrophysical Data, Geochem. Geophy. Geosy., 24, 3, doi:10.1029/2022gc010814.

Githiri, J. G., J. P. Patel, J. O. Barongo and P. K. Karanja (2011). Application of Euler Deconvolution Technique in Determining Depths to Magnetic Structures in Magadi Area, Southern Kenya Rift, J. Agric. Sci. Technol., 13, 1, 1-14, https://ojs.jkuat.ac.ke/index.php/JAGST/article/view/148.

Githiri, J. G., J. P. Patel, J. O. Barongo and P. K. Karanja (2012). Spectral Analysis of Ground Magnetic Data in Magadi area, Southern Kenya Rift, Tanzan. J. Sci., 38, 1, 1-14.

Gloaguen, R., P. R. Marpu and I. Niemeyer (2007). Automatic Extraction of Faults and Fractal analysis from Remote Sensing data, Nonlinear Proc. Geoph., 14, 2, 131-138, doi:10.5194/npg-14-131-2007.

Holden, E., J. C. Wong, P. Kovesi, D. Wedge et al. (2012). Identifying Structural Complexity in Aeromagnetic Data: An Image Analysis Approach to Greenfields Gold Exploration, Ore Geol. Rev., 46, 47-59, doi:10.1016/j.oregeorev.2011.11.002.

Holden, E., P. Kovesi, M. Dentith, D. Wedge et al. (2010). Detection of regions of Structural Complexity within Aeromagnetic Data using Image Analysis, 25th International Conference of Image and Vision Computing New Zealand, 1-8, doi:10.1109/IVCNZ.2010.6148856.

Kodikara, G. R. L., T. Woldai, F. Ruitenbeek, K. Shepherd et al. (2016). Mapping Evaporite Minerals and Associated Sediments in Lake Magadi, Kenya, Using Hyperspectral Hyperion Data, Journal of the University of Ruhuna, 4, 1-2, 22-27, doi:10.4038/jur.v4i1-2.7882.

Komolafe, A. A., Z. N. Kuria, T. Woldai, M. Noomen et al. (2012). Integrated Remote Sensing and Geophysical Investigations of the Geodynamic Activities at Lake Magadi, Southern Kenyan Rift, Int. J. Geophys., 318301, 15, doi:10.1155/2012/318301.

Komolafe, A. A., Z. N. Kuria, T. Woldai, M. Noomen et al. (2013). Investigations into the Tectonic Faults on Magadi Geothermal Field Using Ground and Aeromagnetic Data, Phys. Rev. Res. Int., 3, 4, 385-406, https://journalpsij.com/index.php/PSIJ/article/view/166.

Kuria, Z. N. (2011). Seismotectonics of Active Faults: Magadi Fault System, Southern Kenya Rift, Doctoral dissertation, Ph. D. thesis, Dissertation.

Mariita, N. O. and G. R. Keller (2007). An Integrated Geophysical Study of the Northern Kenya Rift, J. Afr. Earth Sci., 48, 2-3, 80-94, doi:10.1016/j.jafrearsci.2006.05.008.

Minelli, L., A. Vecchio, F. Speranza, I. Nicolosi et al. (2016). Aeromagnetic Investigation of Southern Calabria and the Messina Straits (Italy): Tracking Seismogenic Sources of 1783 and 1908 Earthquakes, J. Geophys. Res. Sol. Ea., 121, 3, 1297-1315, doi:10.1002/2015JB012305.

Muirhead, J. D., S. A. Kattenhorn, H. Lee, S. Mana et al. (2016). Evolution of Upper Crustal Faulting Assisted by Magmatic Volatile Release during Early-stage Continental Rift Development in the East African Rift, Geosphere, 12, 6, 1670-1700, doi:10.1130/ges01375.1.

Nyakundi, E. R., G. J. Gitonga and M. K'Orowe (2021). Simultaneous Modelling of Gravity and Magnetic Data in a measured Heat Flux Area to Characterize Geothermal Heat Sources: A Case for Eburru Geothermal Complex, Kenya, J. Geosci. Environ. Prot., 9, 5, 40-54, doi:10.4236/gep.2021.95005.

Odero, E., J. Githiri and M. K'Orowe (2024). Exploring heat sources using gravimetric data: a case study of Magadi geothermal prospect, Kenya, J. Geosci. Environ. Prot., 12, 5, 147-161, doi:10.4236/gep.2024.125009.

Olafisoye, E. R., N. A. Adegoke and O. A. Alagbe (2022). Geophysical Investigation of the Crustal Structural Framework of Ilesha, Southwestern Nigeria, World J. Adv. Eng. Eng. Technol. Sci., 5, 2, 123-135, doi:10.30574/wjaets.2022.5.2.0052.

Omenda, P. (2014). Geothermal Country Update Report for Kenya: Naivasha, Presented at Short Course IX on Exploration for Geothermal Resources, organized by UNU-GTP, GDC and KenGen, at Lake Bogoria and Lake Naivasha, Kenya, Nov., 2-24.

Omenda, P. A. (2007). The geothermal activity of the East African Rift, Short course II on surface exploration for Geothermal Resources, organized by UNU-GTP and KenGen, at Lake Naivasha, Kenya, 2-17.

Omenikolo, I. A., T. T. Emberga and A. I. Opara (2022). Basement Depth Re-valuation of Anomalous Magnetic Bodies in the Lower and Middle Benue Trough using Euler Deconvolution and Spectral Inversion Techniques, World Journal of Advanced Research and Reviews, 14, 2, 129-145, doi:10.30574/wjarr.2022.14.2.0356.

Owen, R. B., R. W. Renaut and T. K. Lowenstein (2018). Spatial and Temporal Geochemical Variability in Lacustrine Sedimentation in the East African Rift System: Evidence from the Kenya Rift and Regional Analyses, Sedimentology, 65, 5, 1697-1730, doi:10.1111/sed.12443.

Owen, R. B., R. W. Renaut, R. Potts and A. K. Behrensmeyer (2011). Geochemical Trends through Time and Lateral Variability of Diatom Floras in the Pleistocene Olorgesailie Formation, Southern Kenya Rift Valley, Quat. Res., 76, 1, 167-179, doi:10.1016/j.yqres.2011.05.002.

Pratama, A., S. Bijaksana, M. Abdurrachman and N. Santoso (2018). Rock Magnetic, Petrography, and Geochemistry studies of Lava at the Ijen Volcanic Complex (IVC), Banyuwangi, East Java, Indonesia, Geosci., 8, 5, 183, doi:10.3390/geosciences8050183.

Riaroh, D. and W. Okoth (1994). The Geothermal Fields of the Kenya Rift, Tectonophysics, 236, 1-4, 117-130, doi:10.1016/0040-1951(94)90172-4.

Seht, M. I., S. Blumenstein, R. A. Wagner, D. Hollnack et al. (2001). Seismicity, Seismotectonics and Crustal Structure of the Southern Kenya Rift – New data from the Lake Magadi area, Geophys. J. Int., 146, 2, 439-453, doi:10.1046/j.0956-540x.2001.01464.x.

Sequar, G. W. (2009). Neotectonics of the East African Rift System: New Interpretations from Conjunctive Analysis of Field and Remotely Sensed Datasets in the Lake Magadi Area, Kenya, ITC, https://purl.utwente.nl/essays/91635.

Shahsavani, H. (2018). Comparison of a Low-cost Magneto-inductive Magnetometer with a Proton Magnetometer: A case study on the Galali Iron Ore Deposit in Western Iran, Near Surf. Geophys., 17, 1, 69-84, doi:10.1002/nsg.12026.

Simiyu, S. M. and G. R. Keller (1998). Upper Crustal Structure in the Vicinity of Lake Magadi in the Kenya Rift Valley Region, J. Afr. Earth Sci., 27, 3-4, 359-371, doi:10.1016/s0899-5362(98)00068-2.

Srivastava, P., B. J. Murton, L. G. Sant'Anna, F. Florindo et al. (2023). Red Clays indicate Sub-aerial Exposure of the Rio Grande rise during the Eocene volcanic episode, Sci. Rep. Uk., 13, 1, doi:10.1038/s41598-023-46273-y.

Trepil, F., S. Kahoul, O. Uyimwen, A. Eshanibli et al. (2021). Delineation of Structure Elements and the Basement Depth at the Jifara Plain NW Libya using Integration Application of Potential Field Dataset, Acta Geodyn. Geomater, 1, 201, 83-90, doi:10.13168/agg.2021.0006.

Tsepav, M. T. (2020). Centre for Exploration Targeting and Analytic Signal Techniques as Tools for Interpretation of Aeromagnetic Data: Emphasis on Parts of Mid-Niger Basin, Nigeria, Sci. World J., 15, 4, 16-20, https://www.ajol.info/index.php/swj/article/view/203185/191621.

Utama, H. W. (2023). Geothermal Manifestations Linkage with the Siulak Fault Segment in Kerinci, J. Eng. Sci. Res., 5, 1, 41-46, doi:10.23960/jesr.v5i1.133.

Vignaroli, G., A. Pinton, A. Debenedetti, G. Giordano et al. (2013). Structural Compartmentalisation of a Geothermal System, the Torre Alfina Field (Central Italy), Tectonophysics, 608, 482-498, doi:10.1016/j.tecto.2013.08.040.

Werff, H. (2024). An Autonomous Thermal Camera System for Monitoring Fumarole Activity, Sensors, 24, 6, 1999, doi:10.3390/s24061999.

Williams, S., J. Fairhead and G. Flanagan (2005). Comparison of Grid Euler Deconvolution with and without 2D Constraints using a Realistic 3D Magnetic Basement Model, Geophysics, 70, 3, L13-L21, doi:10.1190/1.1925745.

Wiyono, W., S. H. Siombone and S. Maryanto (2022). Gravity and Remote Sensing methods as a solution in identifying Geothermal Reservoirs on Volcanoes, Int. J. Geophys., 1-13, doi:10.1155/2022/9737979.

Zou, Y., D. Maestrelli, G. Corti, C. D. Ventisette et al. (2023). Influence of Inherited Brittle Fabrics on Continental Rifting: Insights from Centrifuge Experimental Modeling and Application to the East African Rift System, Tectonics, 43, 1, doi:10.1029/2023tc007947.

***CORRESPONDING AUTHOR: Evance ODERO**,
Jomo Kenyatta University of Agriculture and Technology, Physics Department, Nairobi, Kenya
e-mail: evance.obonyo@students.jkuat.ac.ke